Spatially resolved ion density measurements in an oxyfuel cutting flame

C. Martin[1], A. Untaroiu, and K. Xu[2]

[1]Penn State University, Altoona College, crm28@psu.edu
[2]Virginia Tech, Department of Mechanical Engineering

July 20, 2020

Abstract

A novel variation of the Langmuir probe for spatially resolved ion density measurements in a dense flowing plasma is presented. The technique uses a spinning disc to rapidly transit a wire probe through the flame. Spatial resolution is accomplished by post processing data collected with many wire locations. The technique resolves ion density with a resolution of 0.5mm in a 3000K atmospheric pressure flame. The oxyfuel cutting torch flame under study is found to have twelve hollow cones with a 1mm base and 4mm height with ion density $3 \times 10^{18}\mathrm{m}^{-3}$ along their surface. The base of the cones form a ring, the inner diameter of which exhibits similarly large ion density, while the outer diameter appears to be weakened by entrained air. The ion densities decay over mm length scales from their peaks in the inner cones to form a semi-homogeneous annulus with ion density on the order $1 \times 10^{17}\mathrm{m}^{-3}$.

1 Introduction

Motivated by the study of ion current physics in an oxyfuel cutting torch flame, this work presents data produced by a novel variation of the Langmuir probe for spatially resolved ion density measurements in a dense flowing plasma. The technique uses an uncooled fine wire probe mounted on

a spinning disc to limit the wire's time in the flame. Spatial resolution is accomplished by accumulating probe current measurements from many wire locations within a measurement plane and computing a single ion density distribution that optimally matches the probe measurements.

1.1 Motivation

It has been proposed that the semiconductor electrical characteristics of the oxyfuel flame could be leveraged for sensing in mechanized oxyfuel cutting applications [1]. The idea is preceeded by a similar techniques in IC engines [2, 3, 4], propulsion systems [5, 6, 7], and especially furnaces [8, 9]. However, the approach to oxyfuel sensing is complicated by the need for a model relating the details of the current-voltage characteristic to physical process parameters [10, 11, 12].

The absence spatial measurements of ion density in this flame has hindered attempts to move away from the empirical fits presented in these works in favor of models derived from transport physics. For example, [11] showed that saturation currents rise quadratically (not linearly) with the gas flow rates. A simplistic model including only convection and ion recombination gave excellent agreement with data. This promotes a view of the flame where ions decline in concentration with distance traveled in the outer cone, but an earlier work [10] used uniform resistivity to argue that the flame ion density is nearly uniform. Reconciling these conflicting views is only one of the potential benefits of a spatial charge density map of the oxyfuel flame.

The present work establishes a method for resolving ion concentration over length scales around .5mm in the high-temperature oxyfuel flame. The device under study in this work is an Oxweld C-67 cutting torch burning methane depicted in Figures 1 and 2. This two-piece tip is comprised of a brass insert inside a copper sleeve. The red preheat channels shown in the model of Figure 1 supply the flame with premixed fuel and oxygen through twelve triangular passages. The green cutting oxygen passage in the center was not used in these tests. The tip has a recess in its center that is needed to stabilize the flame on virtually all but acetylene-burning torches. Further description of the torch in operation is provided in the sources above.

In proper operation, there are twelve intensely luminous conical flame fronts that stabilize in a ring below the ports. These "inner cones" can vary from one to six millimeters in length depending on the flow conditions. In all conditions, they are shrouded in a single long faintly luminous "outer cone",

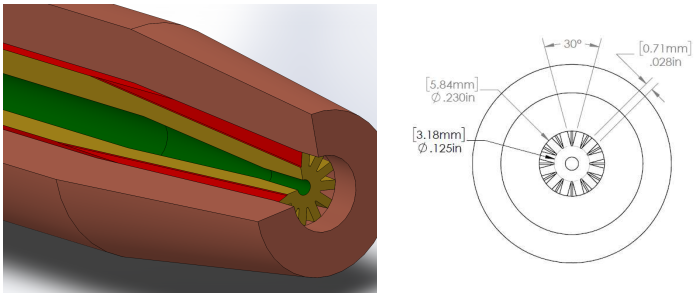

Figure 1: A model and dimensioned drawing of the torch tip used in these experiments.

which can be seen washing over a copper block in Figure 2.

1.2 Ion density measurements

The present state-of-the-art for spatially resolved ion density measurements in flames has been mass spectroscopy for over half a century [13, 14]. Because quenching does not halt the ion recombination reaction or proton exchange, gas sampling tubes must be given up in favor of direct impingment of the flame on the cooled sampling plate of a mass spectrometer [15, 16, 17].

Langmuir probes are merely metal surfaces with an electrical bias inserted into a plasma. The probes need be no more sophisticated than a wire, sphere, or wall, and if the identity of the ion is already known, the local ion densities can be inferred from the measured current. Early measurements using Langmuir probes in flames were performed at low pressures [18], which permitted the use of the sparse plasma theory available at the time [19]. However, the low-density plasma model must be modified in dense "collision-dominated" systems [20, pp.406], and a satisfactory extension of Langmuir probe theory to dense flowing plasmas was not available until the 1970's. Despite their advantages, contemporary use of Langmuir probes in flames is limited, primarily appearing in works extending the probe theory [21, 22, 23]. In this work, we consider two candidate models for estimating ion density from probe measurements offered by Clements and Smy [24, 25].

Temperatures in oxyfuel flames are known to be 3000K or higher [26, 27], which poses a challenge for probe design. Tungsten and platinum alloys are commonly used in high-temperature studies, but at these temperatures

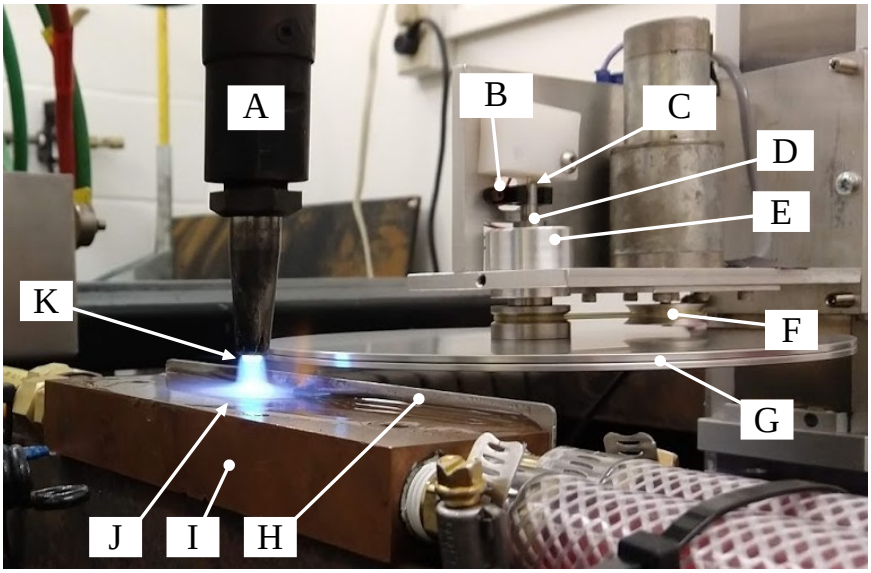

Figure 2: Experimental setup shown in use.

platinum melts and tungsten burns in the presence of oxygen. As a result, measurements in atmospheric flames have historically demanded a probe with active cooling [28]. However, the inner cone of the oxyfuel preheat flame exhibits features on the order of 1mm or smaller, and the diameter of the probe limits the spatial resolution of the measurement. Convective heat transfer to a small cylinder declines slowly with diminishing diameter (like $D^{1/3}$ [29]), while the cooling capacity declines much faster (like D^2), so active cooling always imposes some minimum bulk to the probe.

It is much easier to limit the duration of the probe's exposure to the flame so that there is sufficient time to collect a clear signal but insufficient time for the material to heat to destruction. Clements and Smy used a wire on a spinning disc to artificially simulate high plasma velocities, but it was also demonstrated by MacLatchy as a means of preserving the wire [24, 21]. In these cases, the plasma was presumed to be spatially uniform along the wire's length. The technique presented here is a novel approach to resolving nonuniform ion density resolution along the probe.

2 Approach

The oxyfuel preheat flame's inner cones make its cross section intensely non-uniform with important length scales on the order of 1mm or smaller. Langmuir probes use the current density at the probe's surface to infer the local ion density, but a single current measurement does not allow the experimentalist to reconstruct the distribution of current density along a probe's length in such a flame.

However, the rate of increase of current to a wire probe as it is inserted along its axis could be used to infer the current density at the wire's tip. To ensure that a wire probe survives, the entire process would need to occur in milliseconds. The resulting intense linear acceleration implies a risk of the wire buckling and would inject excessive vibration into the experiment. Also, the analysis would depend on the wire being precisely parallel to the axis of injection.

In the present approach, the probe is a fine wire mounted on a spinning disc so that the wire is made to pass quickly through the flame. Our method for reconstructing the ion density cross-section of the flame is similar to the linear approach above, but with the added complexity that the wire orientation if variable. Consider an initial configuration where the path of the wire allows only the slightest tip of the probe to pass through the flame. The observer could be confident that any measured current was due to ions encountered in the tiny region where the wire tip interacted with the flame's edge. If the disc were then moved by some tiny increment so that the wire is allowed to pass deeper into the flame, whatever current is detected in addition to the previous test could be inferred to have arrived at the probe's tip; now deeper in the flame. If this process were repeated throughout the entire width of the flame, it would be possible to establish a spatially resolved cross-section of the flame's ion density.

2.1 Formulation

We establish a coordinate system shown in Figure 3. Here, the edge of the experiment is imagined to be along the y-axis, so that current to the portions of the probe to the left of the axis ($x < 0$) may safely be assumed to be zero. The center of disc rotation is taken to be $(-d, 0)$, and the wire is presumed to extend a radius, R, from the center along an angle, θ.

When r is the radial distance from the center of the disc along the wire,

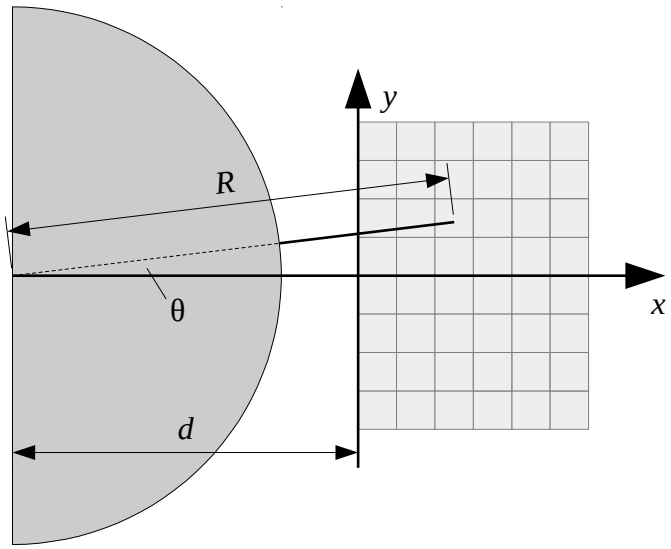

Figure 3: The coordinate system for a single constant-z cross-section of the flame. The location of the probe is defined by the location of the disc center, d, the wire angle, θ, and the probe radius, R.

the measured current on the wire, I, will be an integral of the current per unit length, $\hat{I}_D$,

$$I(d,\theta) = \int_0^R \hat{I}_D(r,\theta)\mathrm{d}r. \tag{1}$$

In this formulation, $\hat{I}_D$ is imagined to be a local property of the plasma that indicates the current per unit length to an absorbing cylinder of diameter, D. If $\vec{X}$ is a vector of values for $\hat{I}_D$ at the nodes of the grid in Figure 3, the problem is establishing values for $\vec{X}$ that best match a series of many data points collected with disc locations d_k and wire locations θ_k.

Regardless of how we choose to interpolate within the elements of the grid, the integral of (1) will reduce to some linear combination of the node values. Therefore, the current to a wire in a specific location, d_k, θ_k, may be expressed as

$$I(d_k,\theta_k) = \vec{\Lambda}(d_k,\theta_k)\cdot\vec{X}. \tag{2}$$

For ease of notation, we will write $I_k = I(d_k,\theta_k)$ and $\vec{\Lambda}_k = \vec{\Lambda}(d_k,\theta_k)$. It

becomes practical to aggregate the error in a least-squares approach.

$$E^2 = \sum_k (I_k - \vec{\Lambda}_k \cdot \vec{X})^2 \tag{3}$$

The values of $\vec{X}$ that minimize this error are calculated by asserting $\partial E^2 / \partial X_n = 0$. This results in the matrix problem

$$\sum_k I_k \vec{\Lambda}_k = \left(\sum_k \vec{\Lambda}_k \vec{\Lambda}_k{}^T \right) \cdot \vec{X}. \tag{4}$$

It remains the responsibility of the experimentalist to collect sufficient data so that the matrix, $\sum_k \vec{\Lambda}_k \vec{\Lambda}_k{}^T$, is not singular. This can be accomplished by collecting data with disc motion increments that are smaller than the grid spacing.

For this work, we adopt a bilinear interpolation scheme to calculate $\vec{\Lambda}$. Inside an element, the value for $\hat{I}_D$ may be calculated

$$\hat{I}_D(x,y) = \phi_{00}(x,y) X_{i,j} + \phi_{10}(x,y) X_{i+1,j} + \ldots \tag{5}$$

$$\phi_{01}(x,y) X_{i,j+1} + \phi_{11}(x,y) X_{i+1,j+1}, \tag{6}$$

where the ϕ functions are the dimensionless bilinear interpolation functions

$$\phi_{00} = \frac{x - x_j}{\Delta} \frac{y - y_i}{\Delta} \qquad \phi_{10} = \frac{x - x_j}{-\Delta} \frac{y - y_{i+1}}{\Delta}$$

$$\phi_{01} = \frac{x - x_{j+1}}{\Delta} \frac{y - y_i}{-\Delta} \qquad \phi_{11} = \frac{x - x_{j+1}}{\Delta} \frac{y - y_{i+1}}{\Delta}$$

when Δ is the uniform grid spacing. Note that though we treat $\vec{X}$ as a vector, we reference it above with two indices. This is a convenient (if somewhat lazy) notation, by which we intend $X_{i,j}$ to refer to the element of $\vec{X}$ corresponding to the node (i,j) in the grid.

Each element only contributes values to four elements of $\vec{\Lambda}$. The element corresponding to the lower-left node is found by integrating ϕ_{00} over the wire path through the element. Similar integrals must be performed for the other three nodes and their corresponding interpolation functions. For each wire position, this process must be repeated for every element through which the wire passes to construct the $\vec{\Lambda}$ vector.

2.2 Experiment

The experiment used a 203mm (8in) diameter aluminum disc with a .254mm (.010in) diameter nichrome wire mounted on a steel shaft in ceramic bearings visible in Figure 2. The bearings were lubricated with a dielectric grease to prevent electrical leakage. A spring-loaded gold-plated pin of the kind used in the inspection of circuit boards was mounted at the center of rotation and brought into contact with the top of the steel shaft, through which the disc was electrified. The gold quickly wore from the surface of the pin, but this was not found to degrade signal quality. The entire assembly was mounted on vertical and horizontal translation stages so that the wire path through the flame could be modified in small increments (on the order .02mm or .001in or smaller).

The finest resolution possible was imagined to be no smaller than one wire diameter. This was imagined to be the smallest scale over which the fluid is undisturbed, but as is discussed in the thin-sheath model proposed by Clements and Smy [25], the ion sampling is not necessarily of the same width as the probe diameter. It may later prove possible to resolve finer grids.

Below the point of electrical contact, the steel shaft was drilled through and a photointerrupter was placed in-line with the hole so that an electrical pulse was generated twice per disc location. When post-processing the results of an experiment, the rising edge of the photointerrupter pulse was used to establish the disc angle at that moment in time. At all points of time between two pulses, the disc location was inferred from constant speed interpolation. Prior to an experiment, angular graduations etched on the disc were used to locate the wire on the disc to the nearest half degree.

The disc rotation was sustained by a urethane belt in a pulley arrangement with a brushed DC motor. The disc speed was controlled manually by changing the voltage applied to the motor and monitored through the photointerrupter pulse frequency. The speed was found to be stationary to better than 0.1% over the course of a two-second test.

Instead of a steel work piece, the torch was positioned over a 12 x 50mm (0.5 x 2in) copper block with 12mm (0.5in) holes drilled along its length. Cooling with a glycol-water mixture in a closed loop with a heat exchanger was effective enough that liquid water can be seen condensing from the combustion products in Figure 2. The same image shows a stainless steel plate was attached to the copper block to deflect the flame away from the disc. In early tests, the flame was allowed to project out under the disc, which heated

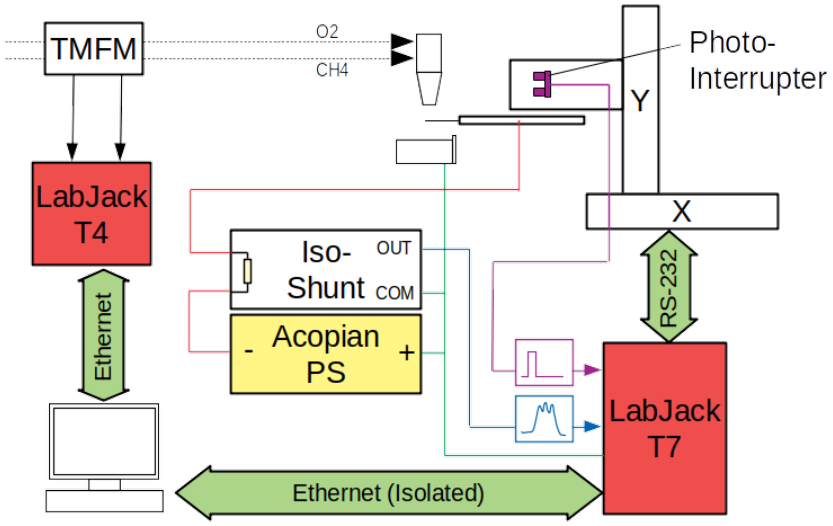

Figure 4: Electrical and fluid connections in the experiment. Thermal mass flow meters are marked "TMFM," and the data acquisition units used are "LabJack" devices.

the aluminum enough to melt the urethane belt.

To prevent corruption from the "wing" of the flame deflected upward towards the wire, horizontal scans were begun with the wire withdrawn beyond the stainless steel deflection plate. While there was signal from this segment of the flame, it was found to be so meager that it did not significantly impact the data.

Figure 4 shows the electrical and fluid connections for the experiment, excluding the cooling system. Oxygen and methane flow rates were monitored by thermal mass flow meters. A low-noise linear power supply was used to apply voltage to the disc through an "iso-shunt" circuit, which was used to transduce the wire current.

The Acopian linear power supply was tuned to bias the system to a negative voltage. By it's design, the isoshunt circuit caused an 8.3% reduction in the excitation voltage, so a -20V excitation would result in -18.3V at the probe. The circuit is shown in the appendix. Prior to each test, a precision $10 \pm .01 \mu$A shunt was shorted at the output of the iso-shunt circuit, and the zero and gain were adjusted appropriately. For most measurements, the system produced 4V per 10μA of probe current.

To scan a single plane of the flame, the disc was inserted and withdrawn in 0.25mm (.010in) increments with a 0.125mm (.005in) offset between insertion and withdrawal. The result is a data set collected with 0.125mm (.005in) increments in wire depth with every other increment collected while either inserting or withdrawing the wire. Additionally, flow rates were recorded before and after each data set. This method was designed to detect hysteresis or drift effects in the data sets.

At each depth, the disc was allowed to dwell for two seconds and data were collected at 50k samples per second. In total, the disc traversed 20mm (.787in), so that scanning a plane resulted in 161 data sets with 100,000 individual measurements in each.

The disc speed was set to approximately 32rad/sec (about 305rpm) by adjusting the voltage applied to the DC motor. The wire tip velocity was approximately 4m/s, leaving the wire immersed in the flame for about 1.5ms. At this speed and sample rate, about 1500 samples were collected per radian of rotation (about 26 per degree). During a two-second test, the disc speed was found to vary with a standard deviations around .004 to .01 rad/sec (.04 to .1 rpm), and the disc speed was seen to drift by about 1 rad/sec during the 8 minutes required to scan the flame cross-section.

The theory of Clements and Smy also dictates that the speed of the undisturbed flow relative to the wire is also critical for determining the wire current. The fluid velocity in the flame is not precisely known, but may be crudely estimated to be about 75m/s based on the known gas flow rates, flame temperature, and cross-section. To verify that the fluid velocity dominated the wire velocity, the disc speed was increased to 42rad/s (400rpm), 84rad/s (800rpm), and 179rad/s (1700rpm) with no measurable change in the magnitude of the wire current.

After over twenty tests conducted under similar conditions, the wire was found to retain its shape and surface character.

3 Results

Here, we present results from seven horizontal scans of the flame with the torch flowing 9.9NL/min (21scfh) of a 0.83 methane-oxygen ratio by volume.

3.1 Raw measurements

The measurements were first processed by transposing the time of each sample into the disc angle using the method described above. Then, all data outside of the range [-0.3, 0.3] radians were discarded, so that only data corresponding to wire locations near the flame were included.

Because of the high sample rate, even after discarding the data far from the flame, the data set is prohibitively large for the analysis proposed above. The data were further reduced by dividing the angle range into bins .0007 radians wide. In each, there were 10 or more samples, from which the mean, median, and standard deviation were recorded.

Figure 5 shows example results of this analysis with the wire fully immersed in the flame at bias voltages from -15 to -50V in 5V increments. Note that each of these includes at least ten full rotations of the disc, so that each line represents ten individual self-consistent data sets collected within two seconds.

Signals were found to be at least 10μA or more. The standard deviation of the currents accumulated in each of the angular bins was mostly less than 0.1μA with 0.3μA being a typical maximum in a scan. We conclude that signal's noise is typically 1% or less, so rejecting random noise is not the experiment's biggest problem. Instead, the system was found to exhibit rare "jumps" in signal due to unsteadiness in the flow, so we became concerned with establishing a digital filter that could reliably reject extreme outliers. For that purpose, we chose the median value of each bin to represent the current at that angle.

3.2 Calculating ion density

Two theories for calculating positive ion density from cylindrical probe measurements in a dense flowing plasma were produced by Clements and Smy; one in which the sheath is thick [24] and one in which the sheath is thin [30, 25]. The same works take pains to demonstrate that diffusion dominated models do not apply in conditions typical to atmospheric flames.

The sparsity of charge is determined by comparing the Debye length against the probe radius. Since the Debye length is much larger than the mean free path, we need only consider

$$\alpha = \frac{2\lambda_D}{D} = \sqrt{\frac{4\epsilon_0 k T_e}{n e^2 D^2}}, \tag{7}$$

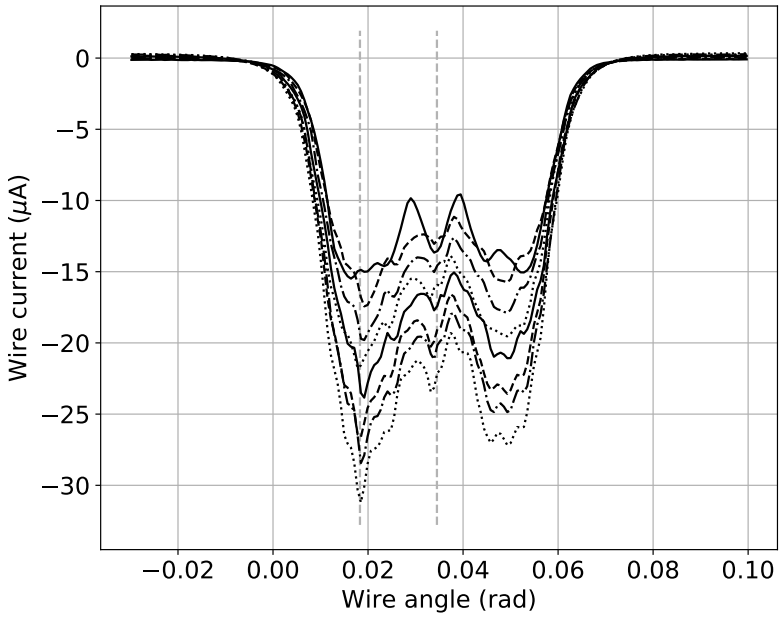

Figure 5: Current signal versus angle for total wire immersion in the flame 3mm from the torch with 9.9L/min and 0.83fuel/oxygen ratio by volume. Bias voltages were from -15 to -50V in 5V increments.

when λ_D is the Debye length, ϵ_0 is the vacuum permittivity, k is Boltzmann's constant, T_e is the electron temperature, n is the density of ions, and D is the probe diameter.

The importance of convection in ratio to diffusion is quantified by the electric Reynolds number,

$$R_e = \frac{UDe}{\mu k T}, \tag{8}$$

where U is the flow velocity, e is the elemental charge, μ is the ion's electrical mobility, and T is the ion temperature.

Finally, the probe bias may be scaled in comparison with the electrical floating potential,

$$\chi = \frac{Ve}{kT_e}, \tag{9}$$

when V is the probe voltage relative to the undisturbed plasma, and T_e is the electron temperature. In this work, we borrow Clements and Smy's approximation that $T_e \approx T$. While crude, this is likely to be a better approximation in chemical plasmas than in arc discharges, where the energy originates in electrons.

The large-sheath model requires that $R_e\alpha^2\chi^2 > 1$, while the small sheath model requires that $R_e\alpha^2 < 1$. Since $\chi \gg 1$ to ensure probe saturation, these conditions overlap. Table 1 shows estimates for the values appropriate to the oxyfuel flame for the H_3O^+ ion based on prior measurements [11].

While these conditions clearly exist partially in a regime where both models may apply, it appears that the large sheath model always applies. Still, the authors caution that the large sheath model is "[...] not in the spirit of the sophisticated treatment given by other authors[...]," so there is good cause for caution. From [24] and [25],

$$V = \frac{\hat{I}^{3/2}}{2neU\sqrt{2\pi\mu\epsilon_0}} \ln\left(\frac{\hat{I}}{neUD}\right) \quad : \quad R_e\alpha^2\chi^2 > 1 \tag{10}$$

$$\hat{I} = 5.3(0.5\epsilon_0\mu D)^{.25}(neU)^{.75}V^{.5} \quad : \quad R_e\alpha^2 < 1. \tag{11}$$

We determine which is more appropriate to the present experiment by comparing the probe current dependence on voltage against the predictions

Table 1: Physical and dimensionless experimental parameters

Parameter		Value	Units
Velocity	U	75	m/s
Ion Mobility	μ	1.1×10^{-3}	m^2/Vs
Temperature	T	3,000	K
Probe Dia.	D	0.254	mm
Ion Density	n	10^{16}-10^{18}	m^{-3}
Debye Len.	λ_D	3.8-38	μm
Voltage	V	15-50	V
	χ	58-190	-
	R_e	68	-
	α	.03-.3	-
	$R_e\alpha^2$	.061-6.1	-
	$R_e\alpha^2\chi^2$	210-230,000	-

made in (10) and (11). The vertical dashed lines in Figure 5 mark wire positions at the current's peak value and at the flame's center. Figure 6 shows the current at these locations with a bias from -15 to -50V in 5V increments.

The extrapolated curves were established by estimating the ion densities at -20V bias and using the respective equations to predict the change with voltage. The data agree well with the thin sheath model. It should also be emphasized that the pedestals of Figure 5 represent self-similar profiles of incrementally increasing amplitude except for data collected with a -15V bias; where a distortion of the data seems to have occurred. This is especially visible in the center line data in Figure 6.

The ion density estimates obtained using this method at -20V bias were within 25% of each other. While that seems to confirm that either model might be applied, we adopt the thin sheath model with a -20V bias. A larger bias would grow the sheath and could reduce the measurement's resolution. A smaller bias would risk the signal deformation we observe at -15V.

3.3 Ion density

Figure 7 shows the post-processing results of the seven planar scans at heights from 1 to 4mm in 0.5mm increments. Positive z was defined as down with

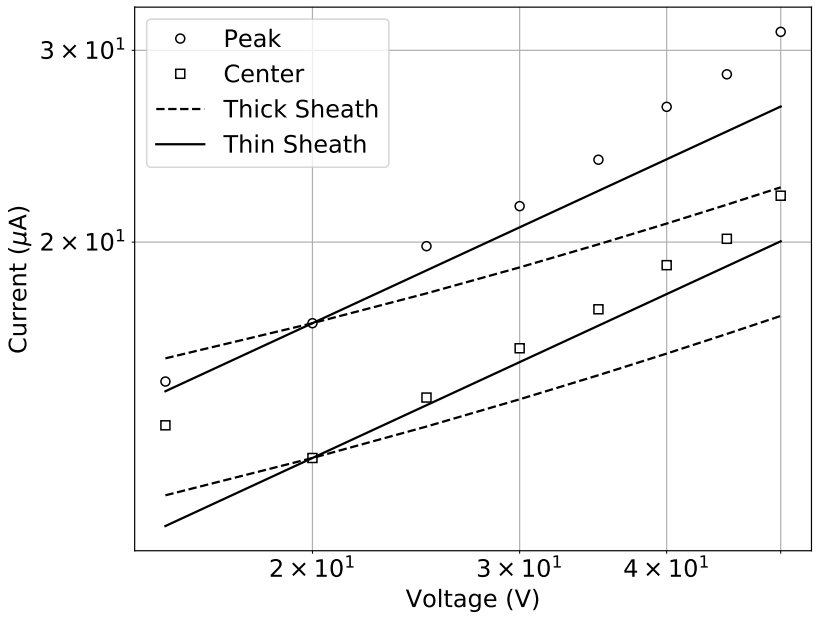

Figure 6: Probe current versus voltage for the two wire angles marked in Figure 5. The solid and dashed lines show extrapolations from 20V bias using (10) and (11)

$z = 0$ corresponding to the height at which the wire was found to barely contact the underside of the torch tip. Like the injection and withdrawal of the wire, these scans were conducted out of order to detect drift or hysteresis in the data.

The grid for the post-processing shown in Figure 7 was 0.25mm uniform spacing; twice the spacing of the wire insertion increments.

4 Discussion and conclusions

The technique is able to resolve the inner cones as hollow cones about 1mm across with ion density around $10^{17}\mathrm{m}^{-3}$ around their base and rising to $3 \times 10^{18}\mathrm{m}^{-3}$ at the tip. The measurements resolved features twice the grid resolution (about .5mm).

4.1 Striping artifacts

There is a series of vertical stripes that are especially prominent in some of the frames of Figure 7. The wave length of these stripes correspond to twice the grid resolution, and appear to be due to poor numerical conditioning.

To rule out artifacts due to the alternating order of data collection (the insertion/retraction order described in Section 2.2), experiments were repeated with sequential wire depths with no noticeable impact on the result. To examine the impact of grid resolution versus data resolution, the post-processing was repeated with lower .5mm grid resolution (Figure 7 has .25mm resolution), but striping artifacts were still present in roughly the same amplitude.

Certainly, it is not a coincidence that the patterns correspond to the direction of wire motion. It seems likely that these stripes are a kind of aliasing due to poor numerical conditioning. We propose to address the issue by applying some additional pre-conditioning to the raw data sets to suppress wave lengths above the grid resolution; not unlike an anti-aliasing filter.

4.2 Experimental Uncertainties

When we examine (11), for the impact of experimental errors on the measurements in Figure 7, we see that ion density is only weakly impacted by wire diameter and ion mobility. Wire diameter is quite precisely known, and

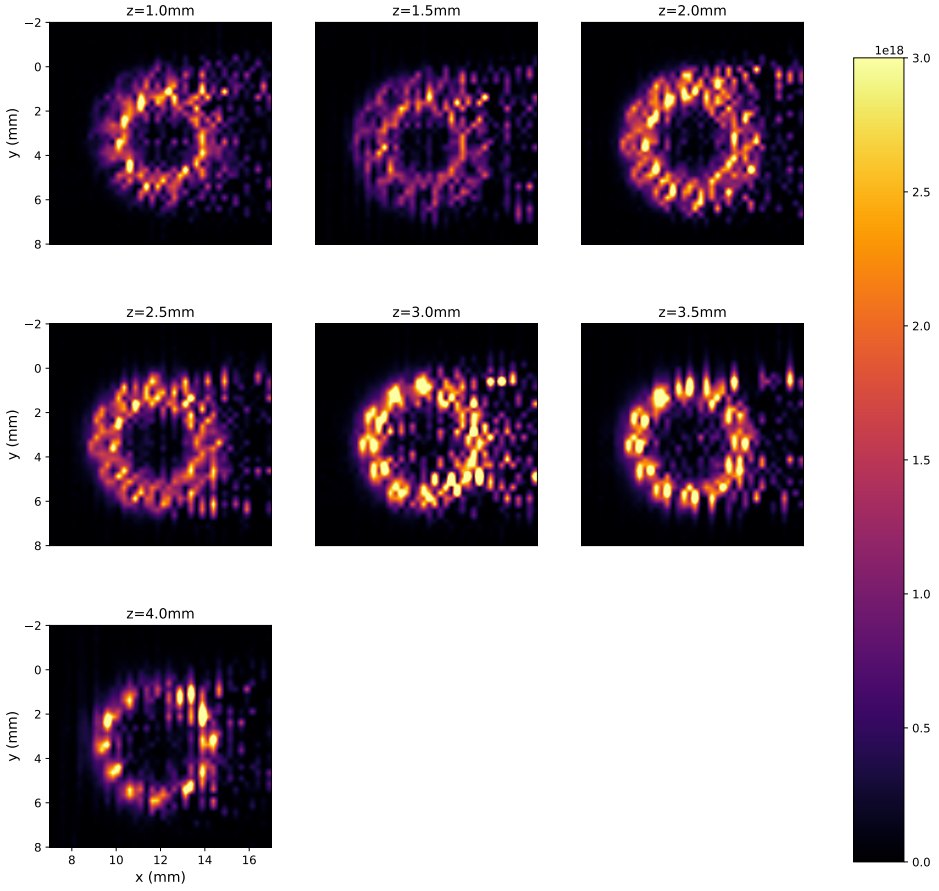

Figure 7: Pseudo-color ion density cross sections. The scale is shown so that the brightest points correspond to $3{\times}10^{18}\mathrm{m}^{-3}$.

the ion mobility has been measured directly [31]. Were mobility to have 5% error, it would only impact ion density by less than 2%. Due to the voltage drop in the iso-shunt circuit, voltage may drop by 5% during an experiment, which could have a 3.3% impact on ion density calculations.

Meanwhile, the value, $U \approx 75$m/s, is estimated from the known gas flow rates, approximate density in the flame, and approximate mean flow area. This number fails to account for local variations in fluid velocity and depends on other parameters that are not carefully determined. We speculate that the actual velocity might vary from 50 to 100m/s with an inversely proportional impact on ion density. If that is so, it dominates all other errors.

There is also reason to examine whether radial components of the gas velocity impact the measurement. If the flow were found to be intense in the radial direction, those flow components would affect the signal differently when the wire was normal to the torch's radius versus at the torch center, causing an elliptical skew in the calculated ion density measurements. Because no such skewing of the data is apparent, we conclude that radial velocity components do not significantly impact the wire signal.

These observations have two impacts on our interpretation of Figure 7. First, the peak ion density might be adjusted as low as $2 \times 10^{18}\text{m}^{-3}$ or as high as $4.5 \times 10^{18}\text{m}^{-3}$. Second, the low densities measured outside of the inner cones might be under-represented since these are regions where the actual velocity may be lower than estimated.

While probe current uncertainties are estimated to be about .01%, it is possible that the striping artifacts may have caused some error in the calculations for $\hat{I}_D$. If that is later discovered to be the case, every 3% error in $\hat{I}_D$, corresponds to approximately 4% error in n.

4.3 Ion density distribution

Experimental uncertainties withstanding, these measurements permit us to say a great deal about the electrical structure of the flame. The inner cones of the oxyfuel flame exhibit hollow cones of intense ion concentration (greater than $10^{18}m^{-3}$). There is a similarly intense ring along the inner diameter of the recess visible in the $z = 1$mm slice, which seems to correspond to the core of a toroidal vortex. The inner cone bases and the outer cone exhibit moderate concentrations of ions (order $5 \times 10^{17}\text{m}^{-3}$ or lower).

The ion mobility is meager enough that diffusion between parallel streamlines may be neglected over mm length scales. Since the streamlines will

convect ions beyond the inner cones, it is clear that ions form in the flame fronts and rapidly recombine over mm length scales in the outer cone.

The weaker density found at the outside edge of the inner cones' bases is likely due to the entrainment of ambient air along the torch tip. This is consistent with the relatively intense ring of ions at the inside of the annulus base. The densities recover along the flame front as distance from the torch tip increases and as the inner cone cross sections decrease.

Only 4mm below the torch tip, the rings of intense ion concentration have faded to form an annulus roughly 6mm in outer diameter with ion density around $10^{17}\mathrm{m}^{-3}$ or lower while only the tips of the inner cones remain. The peak ion concentration has been found to be near $3 \times 10^{18}\mathrm{m}^{-3}$; consistent with the highest ion concentrations reported in flames [20, pp 425].

Acknowledgments

This material is based upon work supported by the National Science Foundation under Grant No. 1900698.

Appendix

The "iso-shunt" circuit used to measure current is appended in Figure 8.

References

[1] C. Martin, "Mechanized oxyfuel control using ion current sensing," *The Welding Journal*, vol. 96, no. 5, pp. 154–162, May 2017.

[2] R. Rao and D. Honnery, "A study of the relationship between NOx and the ion current in a direct-injection diesel engine," *Combustion and Flame*, vol. 176, pp. 309–317, 2017.

[3] T. Badawy, A. Shrestha, and N. Henein, "Detection of combustion resonance using an ion current sensor in diesel engines," *ASME Journal of Engineering for Gas Turbines and Power*, vol. 134, pp. 052 802–1–9, 2012.

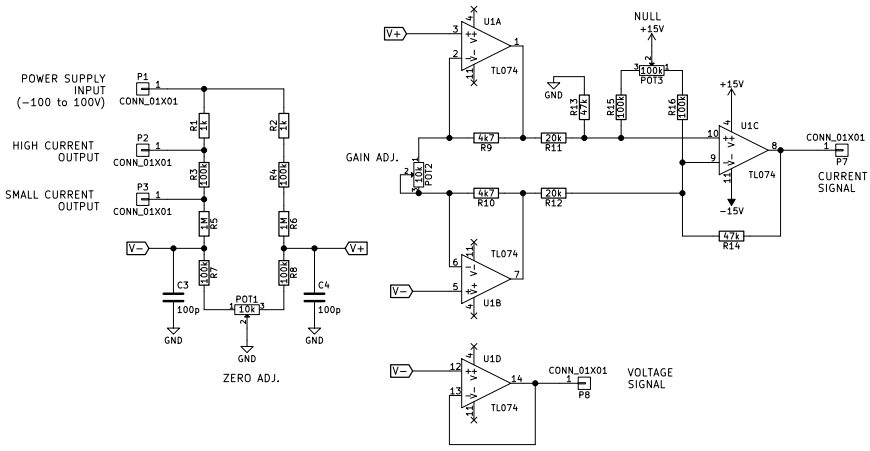

Figure 8: The circuit diagram for the current measurement circuit labeled "isoshunt" in Figure 4

[4] W. G. Rado, "Characteristics of a plasma generated by combustion in a spark ignition engine," *Journal of Applied Physics*, vol. 46, pp. 2468–2474, 1974.

[5] B. T. Chorpening, J. D. Thornton, E. D. Huckaby, and K. J. Benson, "Combustion oscillation monitoring using flame ionization in a turbulent premixed combustor," in *Proceedings of the ASME*, vol. 129, 2007, pp. 352–357.

[6] L. B. W. Peerlings, Manohar, V. N. Komilov, and P. de Goey, "Flame ion generatino rate as a measure of the flame thermo-acoustic response," *Combustion and Flame*, vol. 160, pp. 2490–2496, 2013.

[7] F. Li, L. Xu, M. Du, L. Yang, and Z. Cao, "Ion current sensing-based lean blowout detection for a pulse combustor," *Combustion and Flame*, vol. 176, pp. 263–271, 2017.

[8] A. Jones, "Flame failure detection and modern boilers," *Journal of Physics E: Scientific Instruments*, vol. 21, pp. 921–928, 1988.

[9] Y.-C. Chien, D. Escofet-Martin, and D. Dunn-Rankin, "Ion current and carbon onoxide release from an impinging methane/air coflow flame in an electric field," *Combustion and Flame*, vol. 204, pp. 250–259, 2019.

[10] C. Martin, C. Leonard, and J. VonFricken, "A study of the electrical characteristics of an oxy-fuel flame," *Experimental Thermal and Fluid Science*, vol. 88, pp. 65–72, 2017.

[11] C. R. Martin, "A study of ion currents in an oxyfuel flame due to work surface chemical action," *Experimental Thermal and Fluid Science*, vol. 98, pp. 239–250, 2018.

[12] T. L. Pond and C. R. Martin, "Electrical characteristics of the oxyfuel flame while cutting steel," *Experimental Thermal and Fluid Science*, vol. 112, 2020.

[13] J. Deckers and A. Van Tiggelen, "Ion identification in flames," in *Seventh Symposium on Combustion*, vol. 7. Combustion Institute, 1958, pp. 254–255.

[14] P. F. Knewstubb and T. M. Sugden, "Mass spectrometry of the ions present in hydrocarbon flames," in *Seventh Symposium on Combustion*, vol. 7, no. 1. Combustion Institute, 1958, pp. 247–253.

[15] H. Jones and A. Hayhurst, "Measurements of the concentrations of positive and negative ions along premixed fuel-rich flames of methane and oxygen," *Combustion and Flame*, vol. 166, pp. 86–97, 2016.

[16] A. Hayhurst, J. Goodings, and S. Taylor, "The effects of applying electric fields on the mass spectrometric sampling of positive and negative ions from a flame at atmospheric pressure," *Combusiton and Flame*, vol. 161, 2014.

[17] J. M. Goodings, D. K. Bohme, and T. M. Sugden, "Positive ion probe of methane-oxygen combustion," *Kinetics of Elementary Reactions*, pp. 891–902, 1977.

[18] H. Calcote and I. King., "Studies of ionization in flames by means of Langmuir probes," in *Symposium (International) on Combusiton*, vol. 5, 1955, pp. 423–434.

[19] I. Langmuir, "Studies of electric discharges in gases at low pressures," *General Electric Review*, vol. 27, no. 12, p. 810, 1924.

[20] A. B. Fialkov, "Investigations on ions in flames," *Progress in Energy and Combustion Science*, vol. 23, pp. 399–528, 1997.

[21] C. S. MacLatchy, "Langmuir probe measurements of ion density in an atmospheric-pressure air-propane flame," *Combustion and Flame*, vol. 36, pp. 171–178, 1979.

[22] C. S. MacLatchy and H. C. L. Smith, "The electron current to a langmuir probe in a flowing high-pressure plasma," *IEEE Transactions on Plasma Science*, vol. 19, no. 6, 1991.

[23] P. R. S. James Dawe, Syed A. H. Rizvi, "Electron current to a cylindrical probe in a moving high pressure plasma," *IEEE Trans. on Plasma Sci.*, vol. 21, no. 1, February 1993.

[24] R. M. Clements and P. R. Smy, "Electrostatic-probe studies in a flame plasma," *Journal of Applied Physics*, vol. 40, pp. 4553–4558, 1969.

[25] ——, "Ion current from a collision-dominated flowing plasma to a cylindrical electrode surrounded by a thin sheath," *Journal of Applied Physics*, vol. 41, no. 9, pp. 3745–3749, 1970.

[26] G. Jones, B. Lewis, and H. Seaman, "The flame temperatures of mixtures of methane-oxygen, methane-hydrogen, and methane-acetylene with air," *Journal of the American Chemical Society*, vol. 53, no. 11, pp. 3992–4001, 1931.

[27] N. G. Glumac, "Flame temperature predictions and comparison with experiment in high flow rate, fuel-rich acetylene/oxygen flames," *Combustion Science and Technology*, vol. 122, pp. 1–6, 2007.

[28] H. F. Calcote, "Ion and electron profiles in flames," in *Ninth Symposium on Combustion*, vol. 9. Combustion Institute, 1963, pp. 622–637.

[29] R. Hilpert, "Wärmeabgabe von geheizten drähten und rohren im luftstrom," *Forschung im Ingenieurwesen*, vol. 4, no. 5, pp. 215–224, 1933.

[30] R. M. Clements and P. R. Smy, "Ion current to a spherical probe in a flowing high-pressure plasma under thin-sheath conditions," *Proceedings of the IEE*, vol. 117, no. 8, pp. 1721–1724, 1970.

[31] D. Bradley and S. M. A. Ibrahim, "Determination of positive-ion mobilities and collision cross sections in flame gases using electrostatic probes," *Journal of Physics D: Applied Physics*, vol. 7, pp. 1377–1390, 1974.